ELSEVIER

Polymer Degradation and Stability 79 (2003) 359–368

Polymer Degradation and Stability

www.elsevier.com/locate/polydegstab

Effects of ultraviolet radiation exposure on vinyl ester resins: characterization of chemical, physical and mechanical damage

Andrew W. Signor, Mark R. VanLandingham, Joannie W. Chin*

Polymeric Materials Group, National Institute of Standards and Technology, Gaithersburg, MD 20899, USA

Received 16 July 2002; received in revised form 15 September 2002; accepted 18 September 2002

Abstract

The increased use of fiber-reinforced vinyl ester composites in outdoor applications has led to questions concerning the environmental durability of these materials, particularly as related to UV exposure. In this work, artificial ultraviolet (UV) degradation was carried out on neat vinyl ester matrix specimens using an integrating sphere-based UV exposure chamber. Significant changes were observed in the bulk mechanical properties, surface chemistry, and surface morphology after 1000 and 4000 h of exposure. A transition from slightly ductile to brittle behavior was observed along with a decrease of up to 40% in average strain to failure and a decrease of up to 60% in the average specific toughness after exposure. Changes in the hardness and modulus of the surface after exposure were studied by using an atomic force microscopy (AFM) nanoindentation technique. A significant increase in the apparent hardness of the exposed surface was accompanied by an increase in the apparent modulus of the near-surface region. Morphological changes, including an increase in both the number and size of surface defects on the exposed surface were observed using optical microscopy and tapping-mode AFM. Chemical changes in the exposed surfaces were also observed using Fourier transform infrared- attenuated total reflectance (FTIR-ATR) spectroscopy and x-ray photoelectron spectroscopy (XPS).
Published by Elsevier Science Ltd.

Keywords: Vinyl ester; Ultraviolet (UV) degradation; Integrating sphere; Atomic force microscopy; Nanoindentation; X-ray photoelectron spectroscopy; Fourier transform infrared spectroscopy; Attenuated total reflectance

1. Introduction

In recent years, there has been increasing interest in the use of fiber-reinforced polymer (FRP) composites in building and construction due to the many advantages offered by composite materials. Among these advantages are excellent corrosion and fatigue resistance and high strength-to-weight ratio. However, the outdoor environment contains elements that are destructive to organic polymers, such as moisture, acid rain, temperature cycling, and ultraviolet (UV) radiation. UV radiation, in particular, is known to be highly damaging to organic polymeric materials.

The primary objective of this study was to investigate the chemical and mechanical effects of UV radiation on vinyl ester, a thermosetting polymer commonly used in building and construction applications. Effects of exposure to UV radiation generated by a 1000 W xenon arc source were characterized by tensile testing, atomic force microscopy (AFM), Fourier transform infrared spectroscopy (FTIR), and X-ray photoelectron spectroscopy (XPS). Nanoindentation was performed with the AFM on exposed and unexposed specimens to measure changes in hardness and Young's modulus in the exposed surface. The AFM was also used to monitor changes in the surface morphology at the nanoscale. These mechanical, chemical, and microscopy analyses were used to obtain an understanding of how this resin system degrades under exposure to UV radiation, and to determine the effects of UV exposure on bulk tensile properties.

* Corresponding author. Tel.: +1-301-975-6815; fax: +1-301-990-6891.

E-mail address: joannie.chin@nist.gov (J.W. Chin).

0141-3910/02/$ - see front matter Published by Elsevier Science Ltd.
PII: S0141-3910(02)00300-2

2. Experimental

2.1. Specimen preparation

All specimens were fabricated from Derakane 411-350 PA[1] vinyl ester resin, cured with 0.03 mass fraction methyl ethyl ketone peroxide (MEKP) catalyst and containing 0.0002 mass fraction silicone antifoaming agent. Once formulated, the resin was allowed to cure for 24 h at room temperature followed by a 2 h post-cure at 150 °C. Specimens were prepared in two different forms: ASTM D 638 Type-V tensile specimens (nominally 1.6 mm thick) and 60 mm×60 mm×1.6 mm sheets for AFM and FTIR-ATR analysis. Both specimen forms were manufactured via a modified injection-molding process. In both cases, the mold consisted of a silicone rubber gasket sandwiched between two poly(-methyl methacrylate) platens lined with polyester release film. In the case of the cast sheet, a 60 mm×60 mm opening was cut from the gasket. In the case of the tensile specimens, cavities were punched out of the gasket using an ASTM D 638 Type-V punch. The tensile specimens were produced in groups of six, with each group being produced from the same batch of catalyzed resin. 10 mm×10 mm specimens for AFM, FTIR-ATR, and XPS analysis were cut from the 60 mm×60 mm cast sheet by scoring with a razor blade.

2.2. Ultraviolet radiation exposure

UV exposures were carried out using a 1000 W xenon arc lamp from Oriel Instruments coupled with a 0.3 m diameter integrating sphere, as shown in Fig. 1. An integrating sphere is a hollow spherical chamber that has a highly diffuse reflecting inner surface. The optimal inner surface coating, for UV applications, is fabricated from pressed polytetrafluoroethylene powder or bulk fluoropolymers, both having greater than 98% reflectance at UV wavelengths longer than 280 nm [1]. When radiation enters an integrating sphere, it undergoes multiple, diffuse reflections at the interior surface. After a minimum of two reflections, the radiation inside the sphere becomes spatially integrated, highly uniform, and has an increased irradiance that is directly proportional to the total radiation flux entering the sphere. With proper design, the radiation exiting a port opening in the wall of an integrating sphere is extremely uniform (> 95%) over the dimensions of the port [1].

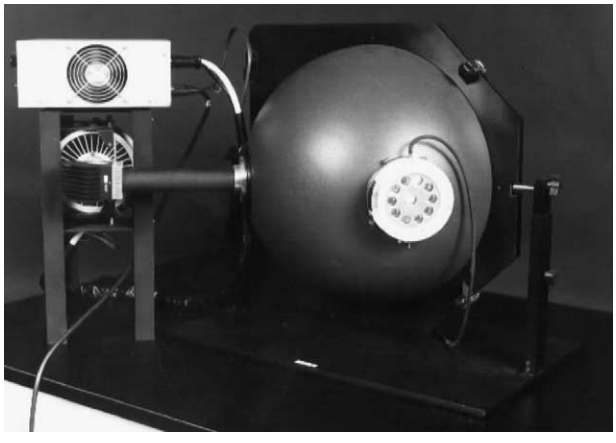

Fig. 1. An integrating sphere-based UV exposure chamber.

The lamp system used in this study contained a dichroic mirror positioned between the xenon bulb and the integrating sphere, which reflected the UV component of the radiation emitted from the lamp into the sphere and transmitted the visible and infrared portions to a heat sink. The use of the dichroic mirror removes the infrared radiation, the primary source of thermal energy in an optical system, and thus limits sample heating. During exposure, the samples were mounted in two 10 cm diameter ports on opposite sides of the integrating sphere.

The UV output was characterized using a Hewlett Packard 8452A spectrophotometer with a diffusing probe; spectra were taken systematically at 33 points across the open area of each port, as shown in Fig. 2(a). This process was used to characterize the spectral irradiance uniformity of the ports and to determine if any irradiance non-uniformity existed either within the individual ports or between the two different ports. All 33 spectra taken on each port exactly superimposed on each other, indicating an extremely high degree of irradiance uniformity over the dimensions of the port. Fig. 2(b) shows the center point spectra from the left and right ports superimposed, indicating that the output of both ports is virtually identical.

The exposure was carried out in an ambient atmosphere where the temperature was nominally between 22 and 24 °C, with a relative humidity between 30 and 50%. A set of control samples that were not exposed to UV was stored in a dark drawer prior to further characterization. A second set of samples was removed from the integrating sphere after 1002 h (hereafter referred to as 1000 h), and a third set of specimens was removed after 3939 h (hereafter referred to as 4000 h) of exposure. The samples were randomized with respect to both exposure time and integrating sphere location in order to minimize any formulation or irradiance non-uniformity effects on data trends.

2.3. Tensile testing

Tensile testing of ASTM D 638 Type-V samples was carried out on a screw-driven Instron 1125 universal

[1] Certain commercial equipment, instruments or materials are identified in this paper in order to specify the experimental procedure adequately. Such identification is not intended to imply recommendation or endorsement by the National Institute of Standards and Technology, nor is it intended to imply that the materials or equipment identified are necessarily the best available for this purpose.

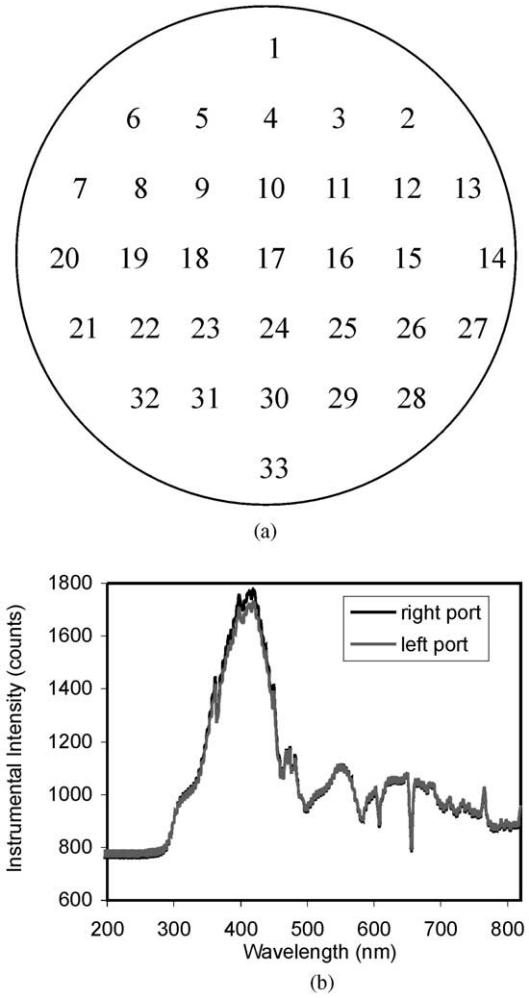

Fig. 2. (a) Spectral analysis points over the plane of the 10 cm diameter exit port on the integrating sphere; (b) comparison of spectral output at the center points (point 17) of the right and left ports of the integrating sphere.

testing machine with manually tightened grips at a constant crosshead speed of 1 mm/min. A torque wrench was used to tighten the grips consistently between samples. Due to the fact that no appropriate extensometer was available, the grip separation was used as the gauge length for measuring extension. A computer software package was used for instrument control, data acquisition, and calculation of all material tensile properties. Engineering stress (σ_e) engineering strain (ε_e), peak load, Young's modulus (although only an estimate due to the lack of extensometer), and specific toughness (energy to break per unit cross-sectional area) were calculated. Nine replicates were tested for both the 1000 and 4000 h specimen sets, while twelve replicates of the control specimens were tested.

2.4. Nanoindentation

Nanoindentation of unexposed controls, 1000 h, and 4000 h specimens was performed using a Digital Instruments Dimension 3100 AFM and Nanoscope 3a controller, and a diamond-tip, stainless steel cantilever probe. A schematic illustration of this AFM system is shown in Fig. 3. For nanoindentation measurements, the AFM is operated in force mode in which, instead of raster scanning the sample surface to produce an image, the probe moves vertically relative to the sample surface to produce a force curve. A force curve is a plot of tip deflection due to cantilever bending, measured using an optical lever system, as a function of the vertical motion of the scanner and can be analyzed to provide information on the local mechanical response [2].

To achieve quantitative AFM nanoindentation measurements, the cantilever spring constant and the probe tip geometry must be determined, and instrumental uncertainties must be limited. In this study, the AFM manufacturer measured the spring constant to be 120 ± 10 N/m using a microbalance technique [2]. Instrumental uncertainties were limited by using small ranges of motion, fast scanner motions, and appropriate calibrations, as described in more detail elsewhere [2]. The most significant of these instrumental uncertainties involves the potential for lateral motion of the probe tip caused by the bending of the cantilever. To limit this effect, a compensating lateral scanner motion was applied that was proportional to the vertical scanner motion, such that the motion of the probe tip would be approximately perpendicular to the sample surface [2]. One way to determine the optimum amount of lateral scanner motion is by performing indentation experiments on a suitably stiff material, e.g. sapphire, such that penetration of the probe tip does not occur. A linear relationship between the tip deflection measured by the photodiode and the force applied to the sample should be achieved. Additionally, this linear relationship is necessary to calibrate the photodiode signal in terms of distance of tip displacement due to bending. The force is then determined from this tip displacement

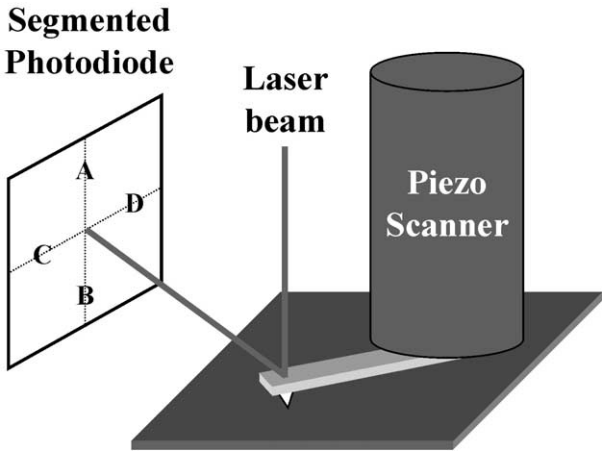

Fig. 3. Schematic illustration of the atomic force microscope (AFM) used in this study.

multiplied by the cantilever spring constant. The penetration of the tip into the sample is then the difference between the vertical displacement of the scanner and the tip deflection.

Finally, to characterize the tip geometry, a method often referred to as blind reconstruction was used [3]. In this method, several "tip characterizer" samples having sharp or other specific features are imaged with an AFM probe, and the shape of the AFM tip is determined from the image data. This tip shape information is then used to generate a relationship between tip cross-sectional area and distance from the tip apex, which are equivalent to contact area and contact depth, respectively, in an indentation experiment. From the tip geometry determined for the diamond-tipped probe, information regarding the contact area, A, was calculated for each indentation experiment using the contact depth, h_c, achieved at the maximum loading point [3]:

$$h_c = h_{max} - \frac{\varepsilon P_{max}}{S} \quad (1)$$

where:

ε = constant related to contact geometry (chosen to be 0.75 [3])
h_{max} = maximum penetration depth
P_{max} = maximum load

To calculate h_c and subsequently elastic modulus, E, a linear estimation of the slope, S, called the contact stiffness, was conducted using the first 10 data points of the unloading curve, as shown in Fig. 4. The relationship between S, E, and A from is given by [3]:

$$S = 2\beta\left(\frac{E}{1-\nu^2}\right)\left(\frac{A}{\pi}\right)^{\frac{1}{2}} \quad (2)$$

where:

β = correction for non-circular contact areas ($\beta = 1.034$ for triangular area)
ν = Poisson's ratio of sample

Thus, values of E can be calculated from the values determined for A and S and using an estimation of ν.

Indentation was carried out using four different maximum forces; data analysis is presented here only for the smallest force used, which was approximately 3630 nN. Arrays of multiple indents were created at different locations until a significant sampling of the entire 1 cm^2 specimen area was obtained.

2.5. Surface morphology

Exposed and unexposed surfaces were studied using the same AFM instrumentation used for nanoindentation. In addition to the diamond-tipped steel cantilever, silicon cantilevers were used to generate tapping-mode AFM images [4]. In tapping mode, the cantilever tip is oscillated at its fundamental frequency, which was approximately 60 kHz for the stainless-steel cantilever and 300 kHz for the silicon cantilevers. The oscillating probe is raster-scanned across the surface while a feedback loop between the vertical scanner and the optical lever system is used to maintain a constant oscillation amplitude. Tapping mode AFM was used to collect height and phase contrast images with scan sizes ranging from 1 μm ×1 μm to 100 μm ×100 μm. Also, optical micrographs of both exposed and unexposed surfaces were obtained using the optical microscope integrated into the AFM system. As with the indentation measurements, microscopy images were taken in several locations in order to obtain a significant sampling of the changes induced by UV exposure.

2.6. Chemical analysis

2.6.1. Fourier transform infrared analysis

FTIR analysis of exposed and unexposed vinyl ester epoxy resin surfaces was performed using a Nicolet Magna-IR 560 spectrometer with an ASI attenuated total reflectance (ATR) probe. The probe consisted of a zinc selenide focusing element and a diamond internal reflectance element. The probe geometry provided three reflections on the sample surface at an angle of incidence, θ, of 45°. The probe was brought into direct contact with the sample surface using light mechanical pressure. 32 scans were collected and co-added over the spectral range of 400–4000 cm^{-1}. Three to four spectra were taken on each specimen.

Both the probe and bench were purged with dry air and background spectra were collected before each sample spectrum was taken. The depth of penetration of the beam into the sample surface, D_p, as a function of wavelength, λ, was estimated with the following equation [5]:

$$D_p = \frac{\lambda}{2n_1\pi\left(\sin^2\theta - n_{21}^2\right)^{\frac{1}{2}}} \quad (3)$$

where:

λ = wavelength
θ = angle of incidence
n_1 = refractive index of sample
n_2 = refractive index of internal reflectance element
n_{21} = $\frac{n_2}{n_1}$

The refractive index of the sample, n_1, was estimated to be 1.5 and the refractive index of the diamond internal reflectance element, n_2, is 2.4.

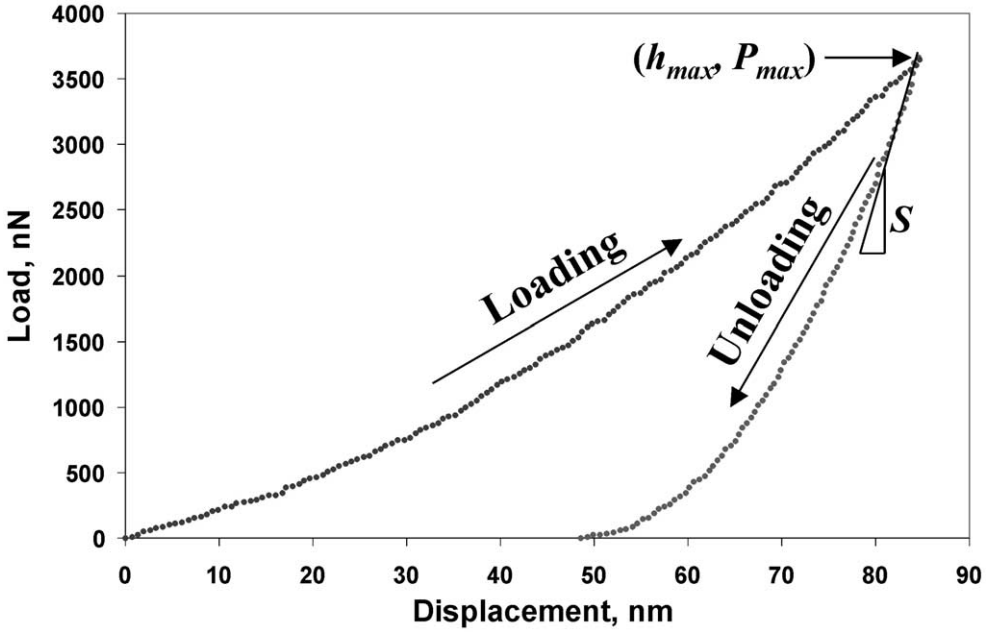

Fig. 4. Representative nanoindentation load (P) vs. displacement (h) curve for vinyl ester.

2.6.2. X-ray photoelectron spectroscopy

X-ray photoelectron spectroscopy (XPS) analysis was carried out on a Perkin-Elmer PHI 5400 spectrometer equipped with a Mg K_α achromatic X-ray source (1253.6 eV), operating at 14 keV and 300 E with an emission current of 25 mA. Pressure inside the ultra high vacuum chamber was maintained around 10^{-6} Pa during the course of analysis. Dimensions of the analyzed areas were typically 1.1 mm $\times$3.3 mm.

Binding energies for all observed photopeaks were referenced to the value of the carbon-carbon/carbon-hydrogen bond at 285.0 eV. Atomic concentration calculations and curve fitting were carried out using PHI software version 4.0.

3. Results and discussion

3.1. Tensile testing

Stress–strain curves for specimens tested after 0, 1000, and 4000 h of exposure are presented in Fig. 5(a)–(c). The unexposed material exhibited slightly ductile behavior, displaying a yield point and a small degree of plastic deformation. Little, if any, statistically significant changes in the tensile properties were observed after 1000 h of exposure; the stress-strain curves still exhibited yielding and plastic deformation. However, after 4000 h of irradiation, there was a distinct transition from ductile to brittle behavior, as shown by the shape of the stress-strain curve. Average strain to failure, tensile strength, modulus and specific toughness are summarized in Table 1. The average ultimate engineering strain decreased from 16.7% for the unexposed material to 14.9% after 1000 h of exposure and 8.9% after 4000 h. The average specific toughness (total energy to break/unit cross-sectional area) decreased from 1.4 kg mm/mm^2 for the unexposed material to 1.2 kg mm/mm^2 after 1000 h of exposure and 0.56 kg mm/mm^2 after 4000 h. This decrease in specific toughness and strain to failure following UV exposure is graphically represented in Fig. 6. Thus, after 4000 h of exposure, the strain to failure decreased to approximately 40% of the original value and the specific toughness decreased to approximately 60% of the original value.

All of the observed changes in tensile properties indicate a transition from ductile to brittle behavior as a result of increasing UV dosage. Specific toughness and ultimate strain were observed to be the most sensitive to UV-induced degradation. Significant embrittlement of, or the creation of additional defects in, a thin surface layer could have significantly reduced the energy required for a crack to nucleate and propagate through the bulk material. Thus, the observed change in bulk properties could actually be a result of the change in the mechanical properties of a thin UV-degraded surface layer. As has been shown by other researchers, the surface cracks in UV-degraded polymers are easily formed and could lead to decreased mechanical properties [6]. Nanoindentation results, to be discussed in the following section, will serve to support or disprove this hypothesis.

3.2. Nanoindentation

A representative load vs. penetration curve for the vinyl ester specimen is shown in Fig. 4, and a summary

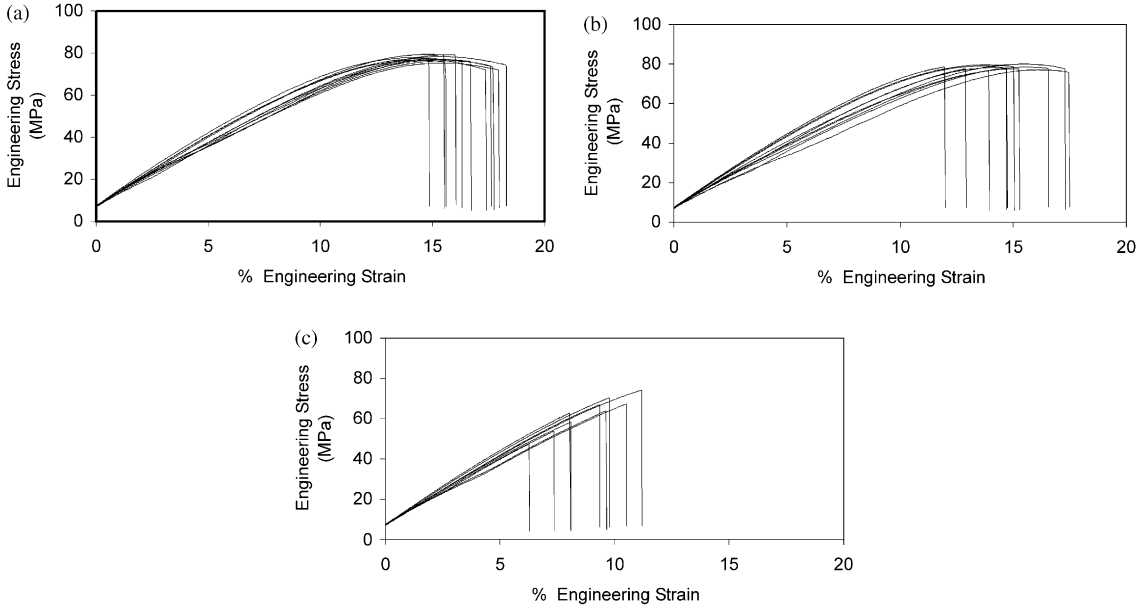

Fig. 5. Stress–strain curves for vinyl ester exposed to UV for (a) 0 h, (b) 1000 h, and (c) 4000 h.

Table 1
Tensile properties of UV-exposed vinyl ester specimens

Exposure time (h)	Ultimate ε_e (%)	E (MPa)	Peak σ_e (MPa)	Specific toughness (kg mm/mm^2)
0	16.72±1.14[a]	654.67±47.57	77.44±1.22	1.44±0.15
1000	14.98±1.78	692.28±71.39	78.24±1.10	1.26±0.19
4000	8.92±1.59	696.67±50.53	62.80±8.38	0.56±0.16

[a] Uncertainties are represented by one standard deviation.

of average modulus (E) values and average maximum penetration (h_{max}) values, as well as the respective standard deviations, is given in Table 2 for a maximum applied load of approximately 3630 nN. An accurate estimate of modulus was difficult to obtain due to the contributions of elastic, plastic, and, in particular, viscoelastic deformation [3]. The modulus values reported here are most useful as relative measures to indicate any changes in the surface mechanical response with UV exposure. Likewise, the values of maximum penetration, which is inversely related to hardness, are also useful as relative measurements.

As shown in Table 2, a decrease in maximum penetration depth (increase in hardness), as well as an increase in the estimated modulus, occurred after 1000 h of exposure. After 4000 h of UV exposure, no indication of further change was observed, taking into consideration the uncertainty in the measurements. Thus, after 1000 h of exposure (or earlier), no further change in the surface modulus or hardness occurs, suggesting that the degradation layer has grown deeper than the average indent depth of about 80–90 nm.

These results are in agreement with studies in which growth of the degradation layer has been reported to reach depths greater than 100 μm in short amounts of time [7]. An increased hardness and modulus at the exposed surface is indicative of embrittlement upon irradiation, which is consistent with the observed bulk tensile properties. Microhardness measurements taken on glass fiber-reinforced polyester composites [8] and epoxy coatings [9] that had undergone UV weathering showed that the surface microhardness increased considerably following 1000 and 800 h of exposure, respectively. Nanoindentation studies on UV-exposed polyvinyl chloride (PVC) have also shown that the surface region had a significantly higher hardness than the bulk, whereas the surface modulus was much less affected [10].

3.3. Surface morphology

Several observations were made concerning morphological changes on the surface of the material upon irradiation. The first was that of macroscopic loss of gloss. The exposed surfaces exhibited less specular reflectance than the unexposed surfaces, and the interface between exposed and unexposed portions of both the 1000 and 4000 h specimens (where a portion of each specimen was shielded from the light by the mount) could be identified with the naked eye. Representative optical micrographs showing the evolution of defects on the surface of the resin with increasing UV dosage are shown in Fig. 7. The unexposed control surface is shown in Fig. 7(a), and the surface after 1000 h of exposure is shown in Fig. 7(c). Fig. 7(b) shows the interface between the exposed and unexposed surfaces

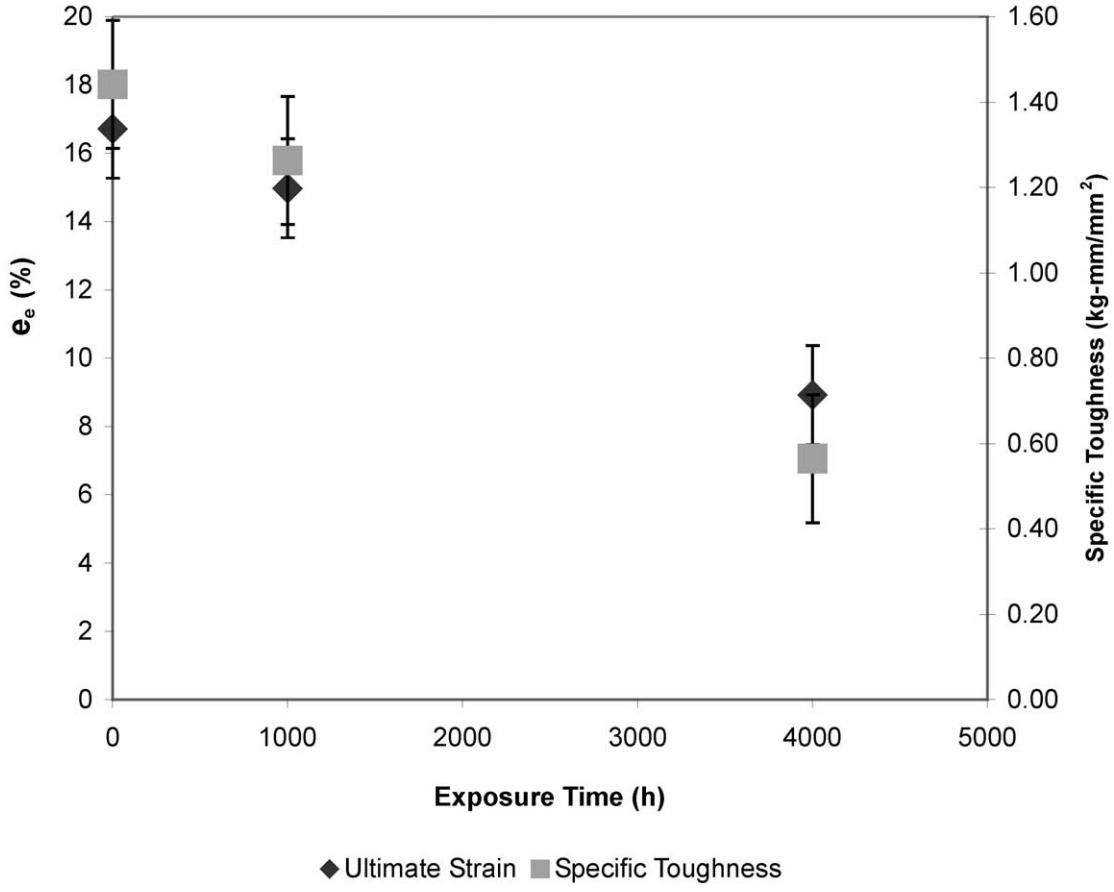

Fig. 6. Ultimate strain and specific toughness of vinyl ester as a function of UV exposure time (error bars represent ± one standard deviation).

Table 2
Nanoindentation data for UV-exposed vinyl ester

Exposure time (h)	Indentation depth (nm)	$E_{estimated}$ (MPa)
0	81.98 ± 8.60[a]	1.23 ± 0.47
1000	51.97 ± 6.89	3.75 ± 1.32
4000	55.71 ± 5.16	2.32 ± 0.64

[a] Uncertainties are represented by one standard deviation.

of the 1000 h specimen that could be discerned with the naked eye.

As the pits and blisters increased in size and number, the scratch-like defects observed in the unexposed specimens disappeared with increasing exposure time, suggesting that localized flow in the surface regions or ablation may have occurred as a result of UV exposure. After 4000 h, the size and number of pits continued to increase and large bull's eye-like and crosshatched defects on the order of 50–100 μm were observed with the optical microscope, as is seen in Fig. 7(d). It has been postulated that during the UV irradiation of polymers, volatile degradation products are removed from the specimen surface, leaving behind pit or pore-type structures [11]. These surface features could accelerate further degradation by providing pathways for oxygen diffusion into the specimen bulk.

Tapping mode AFM using a silicon cantilever revealed the presence of protruding, blister-like features on the order of 10 nm in diameter, with a few of these features reaching heights of 300 nm after 1000 h of exposure. The evolution of these defects on the surface is depicted in Fig. 8. After 4000 h of exposure, the number and size of these protruding defects on the surface increased significantly, nearly all of them reaching a height of about 300 nm. After 4000 h of exposure, the density and size of these features fluctuated little across the entire exposed surface. These features could be due either to the accumulation of degradation products or to the ablation of the surface by the UV degradation. Similar protrusions were observed in the AFM analysis of UV-exposed clear coats [12].

3.4. X-ray photoelectron spectroscopy

Specimens exposed to UV irradiation for 1000 h showed significant changes in the surface chemical composition. Table 3 lists atomic concentrations of carbon, oxygen and silicon found in the vinyl ester films before and after UV exposure. Vinyl ester surfaces are

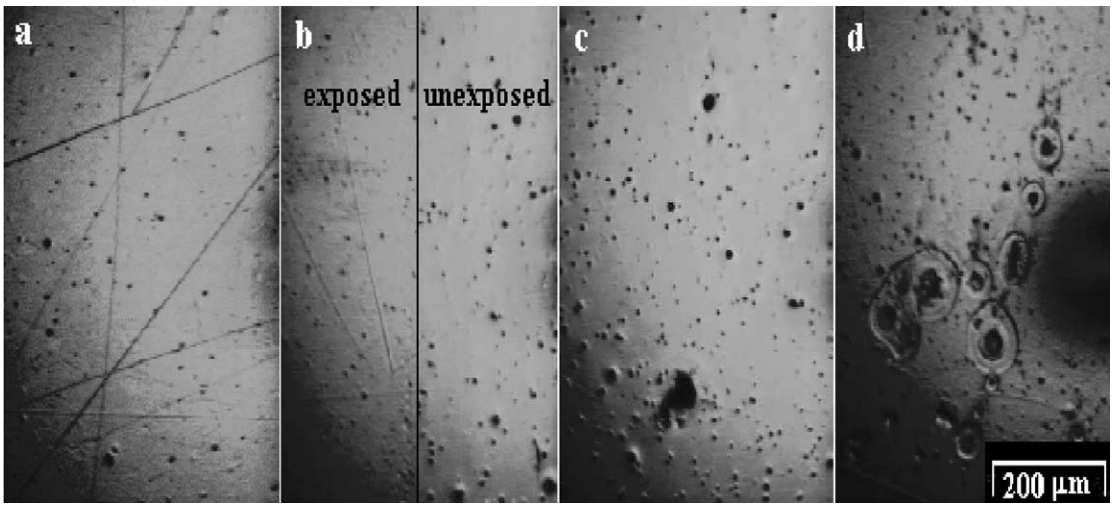

Fig. 7. Optical micrographs of vinyl ester surface after (a) 0 h, (b) 1000 h at interface between unexposed and exposed surfaces, (c) 1000 h, and (d) 4000 h of exposure.

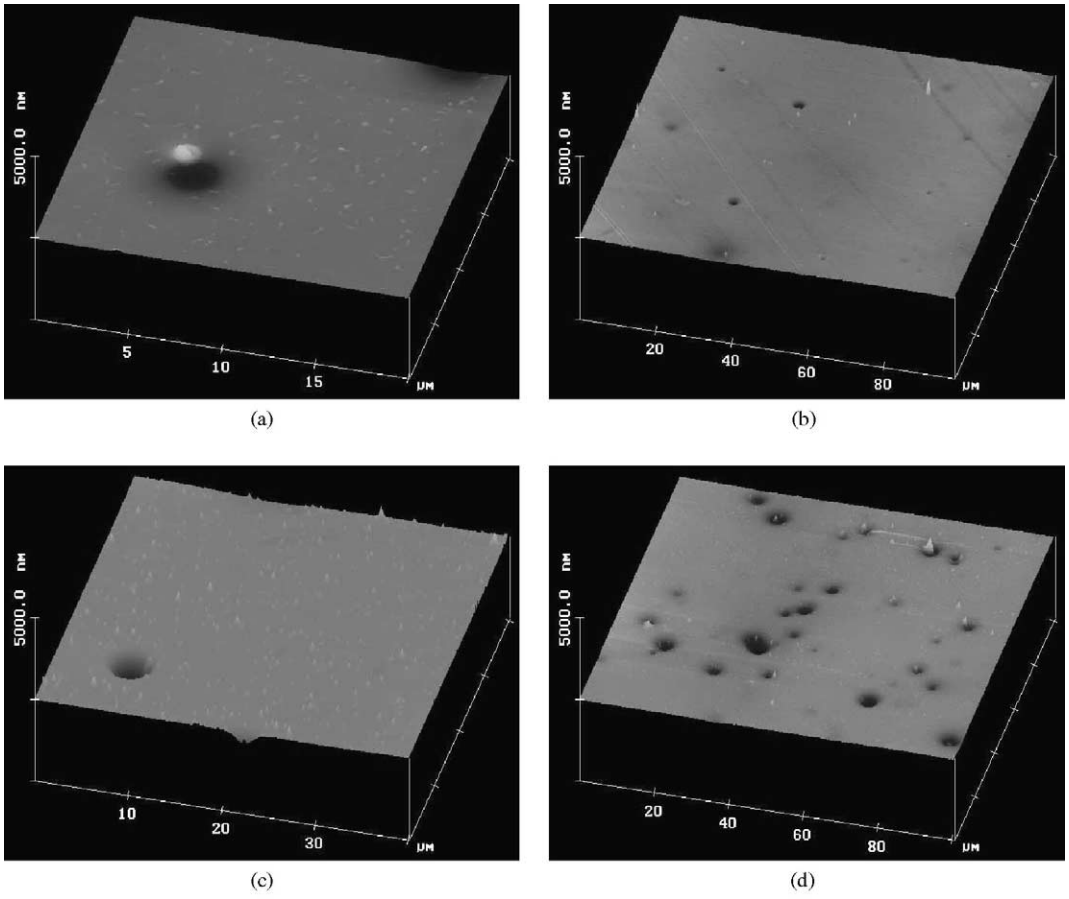

Fig. 8. AFM tapping-mode images of vinyl ester surface after (a) 0 h, (b) 1000 h, (c) 1000 h, and (d) 4000 h of UV exposure.

primarily composed of carbon and oxygen; a small amount of silicon that originates from the silicone defoamer used in specimen preparation is also observed. Following UV exposure, the atomic concentration of oxygen increased from 18.0 to 29.5 at.%. The surface silicon concentration was also observed to increase, possibly due to the ''blooming'' of the silicone defoamer from the bulk up to the surface regions. No further changes were observed in the XPS analysis of the specimens exposed to UV for 4000 h. Since XPS is typically sensitive to the topmost 5–10 nm of a polymeric material, this observation infers that the depth of UV

Table 3
X-ray photoelectron spectroscopy (XPS) atomic concentrations for non-exposed vinyl ester and vinyl ester exposed to UV for 1000 h (standard uncertainty is ±2 at.%)

	Atomic concentration (at.%)		
	Carbon 1s	Oxygen 1s	Silicon 2p
Vinyl ester—non-irradiated	73.3	18.0	8.7
Vinyl ester—UV-irradiated	51.3	29.6	19.1

damage has reached or exceed 10 nm at or prior to 1000 h of exposure. In an XPS study of UV-irradiated polyester, no additional changes in atomic concentration were observed after 100 h [13].

As shown in Fig. 9(a), the curve-fitted carbon 1s photopeak prior to exposure can be fitted with a hydrocarbon peak at 285 eV and two smaller peaks at 286.8 and 289.2 eV, corresponding to C–O and O=C–O, respectively. These functional groups are attributed to the ester linkages in the original vinyl ester network. Following UV exposure, the concentrations of C–O and O=C–O moieties (as shown by their peak heights) increase relative to the main hydrocarbon (C–H) peak. However, when the absolute quantities of C–O and O=C–O linkages are calculated as a function of the total atomic concentration of carbon, it is observed that the concentration of C–O linkages has decreased at the expense of the O=C–O concentration. This result indicates that the C–O moieties, along with some of the hydrocarbon species, have been further oxidized to ester or carboxylic acid linkages. The fact that no increase in C–O was observed could be evidence that the C–O species in vinyl ester that result from UV irradiation is particularly susceptible to further photo-oxidation and has a short lifetime in the presence of UV.

3.5. Fourier transform infrared spectroscopy

The penetration depth of the infrared beam into the vinyl ester surface as calculated in Eq. (3) is graphically depicted in Fig. 10. In the wavelength region of interest, the infrared signals obtained are estimated to originate from the top 3–5 μm of the sample. Fig. 11 shows representative FTIR-ATR spectra for the unexposed specimens and specimens following 1000 and 4000 h of exposure. After 1000 h of exposure, the average peak height of the characteristic ester carbonyl absorption peak at 1727 cm^{-1} increased from 0.02 absorbance units to 0.1 absorbance units, an increase of 400%. Variability in peak heights in FTIR-ATR is typically less than 1%. This increase in carbonyl content at the surface, typically observed in the infrared spectra of polymers following UV photo-oxidation [7,14,15], is consistent with the results of the XPS analysis. No additional increase in the height of the peak at 1727 cm^{-1} was observed at 4000 h. A slight broadening of the peak at

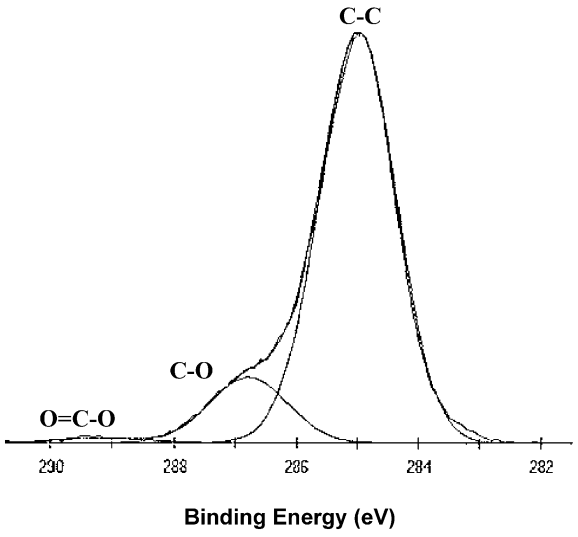

(a)

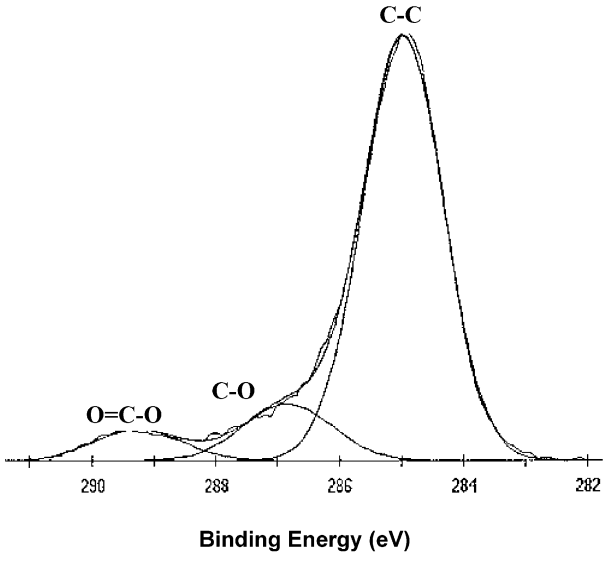

(b)

Fig. 9. Comparison of curve-fitted carbon 1s photopeaks for vinyl ester samples: (a) prior to UV exposure, and (b) following 1200 h of UV exposure.

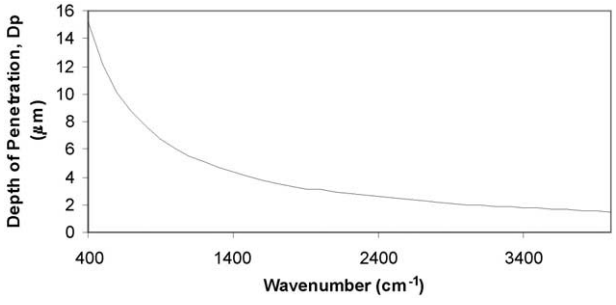

Fig. 10. Depth of penetration of infrared beam in attenuated reflectance mode into vinyl ester surface as a function of wavelength.

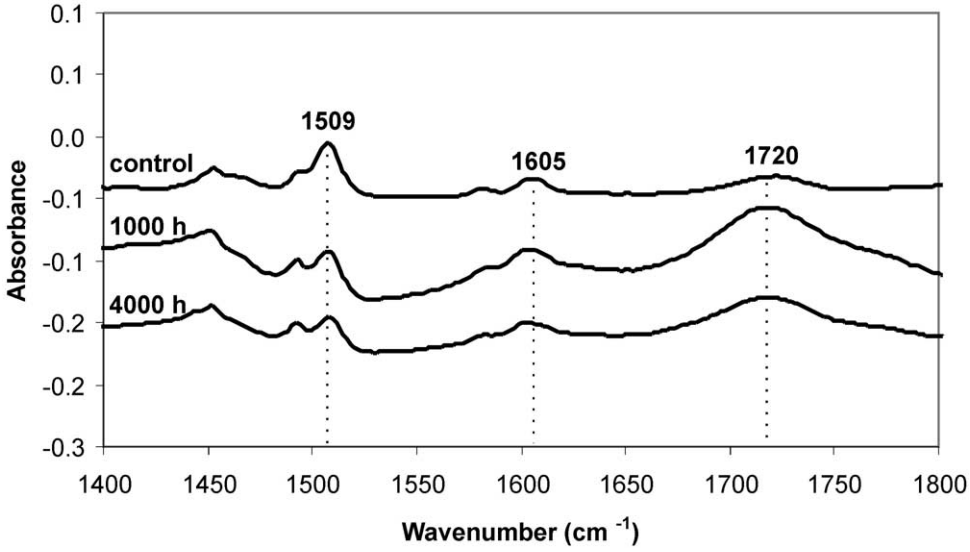

Fig. 11. Representative FTIR-ATR spectra of unexposed vinyl ester, and vinyl ester exposed for 1000 and 4000 h.

1605 cm^{-1}, and a decrease in relative intensity of the peak at 1509 cm^{-1} was also observed for both the 1000 h and the 4000 h specimens. Both of these peaks are associated with the aromatic ring structure.

4. Summary

Exposure to UV radiation can significantly affect the bulk tensile properties of a vinyl ester resin matrix. The ultimate tensile properties such as ultimate strain and specific toughness were sensitive to degradation, with up to a 40% decrease in the ultimate strain and a 60% decrease in specific toughness after 4000 h of exposure in an integrating-sphere-based exposure chamber. The hardness and modulus, as measured by an AFM indentation technique, both increased after 1000 h of exposure, but no significant difference was observed between the 1000 and 4000 h specimens. Both XPS and FTIR-ATR analysis showed evidence of an oxidative photodegradation process, with changes observed for samples exposed for 1000 h but no additional changes in samples exposed for 4000 h. Thus, the surface sensitive measurements all revealed changes for early exposure times. Additionally, pits and protruding features grew in number and size with exposure. Thus, the degradation and embrittlement of the surface, as indicated by the increases in surface modulus and hardness, coupled with an increase in the size and population of surface flaws might have reduced the energy required to nucleate and propagate a crack in tension. Thus, while the degradation may have been limited to a thin surface layer, bulk mechanical properties were significantly affected.

Acknowledgements

The authors would like to thank Eric Byrd and Ned Embree of NIST, and Frank Cromer of the Chemistry Department at Virginia Tech, for their assistance in this research.

References

[1] Martin JW, Chin JW, Byrd WE, Embree E, Kraft KM. Polym Degrad Stab 1999;63:297.
[2] VanLandingham MR, McKnight SH, Palmese GR, Elings JR, Huang X, Bogetti TA, et al. J Adhesion 1997;64:31.
[3] VanLandingham MR, Villarrubia JS, Guthrie WF, Meyers GF. In: Tsukruk V, Spencer ND, editors. Macromolecular Symposia, Recent Advances in Scanning Probe Microscopy of Polymers, 2001. p. 15.
[4] Raghavan D, Gu X, Nguyen T, VanLandingham M, Karim A. Macromolecules 2000;33:2573.
[5] Luoma GA, Rowland RD. J Appl Polym Sci 1986;32:5777.
[6] Fairgrieve SP, MacCallum JR. Polym Degrad Stab 1985;11:251.
[7] Schoolenberg GE, Vink P. Polymer 1991;32:432.
[8] Choi NS, Takahashi K, Oschmann D, Karger-Kocsis J, Friedrich K. J Mater Sci 1998;33:2529.
[9] Bartolomeo P, Irigoyen M, Aragon E, Frizzi MA, Perrin FX. Polym Degrad Stab 2001;72:63.
[10] Turnbull A, White D. J Mater Sci 1996;31:4189.
[11] Kaczmarek H. Polymer 1996;37:189.
[12] Osterhold M, Glockner P. Prog Org Coatings 2001;41:177.
[13] Jian SZ, Lucki J, Rabek JF, Ranby B. In: Proceedings of the 187th Meeting of the American Chemical Society 1985, ACS Symposium Series on Polymer Stabilization and Degradation. p. 353.
[14] George GA, Sacher RE, Sprouse JF. J Appl Polym Sci 1977; 21:2241.
[15] Dubois D, Monney L, Bonnet N, Chambaudet A. Composites Part A: Appl Sci Manufact 1999;30:361.